Finite range corrections near a Feshbach resonance and their role in the Efimov effect

P. Dyke, S. E. Pollack, and R. G. Hulet,

Department of Physics and Astronomy and Rice Quantum Institute,

Rice University, Houston, Texas 77005, USA

(Dated: February 4, 2013)

Abstract

We have measured the binding energy of ^{7}Li Feshbach molecules deep into the non-universal regime by associating free atoms in a Bose-Einstein condensate by modulating the magnetic field. We extract the scattering length from these measurements, correcting for non-universal short-range effects using several different methods. We find that field-dependent effective range corrections agree well with the data. With this more precise determination of the scattering length vs. field we reanalyze our previous data on the location of atom loss features produced by the Efimov effect [1] and investigate effective range corrections to universal theory.

Efimov showed more than 30 years ago that three particles interacting via resonant two-body interactions could form an infinite series of three-body bound states if the two-body s-wave scattering length a could be varied [2]. In the limit of zero-range interactions, the ratios of scattering lengths corresponding to the appearance of each bound state was predicted to be a universal constant, equal to approximately 22.7. The only definitive observations of the Efimov effect have been in ultracold atoms, where the ability to tune a via a Feshbach resonance [3, 4] has proven to be essential. Since the first evidence for Efimov trimers was obtained in ultracold Cs [5], experiments have revealed both three- and four-body Efimov states in several atomic species. Although the Efimov effect has now been confirmed, several open questions remain, including a full understanding of the role of non-universal finite range effects. Accurate comparisons with theory require that these non-universal contributions be quantitatively determined and incorporated.

We previously characterized the $F = 1, m_F = 1$ Feshbach resonance in ^{7}Li, which is located at approximately 737 G, by extracting a from the measured size of trapped Bose-Einstein condensates (BEC) assuming a mean-field Thomas-Fermi density distribution [1, 6]. These data were fit to obtain $a(B)$, the function giving a vs. magnetic field, which was used to assign values of a to Efimov features observed in the rate of inelastic three- and four-body loss of trapped atoms [1]. More recently, two groups have characterized the same Feshbach resonance by directly measuring the binding energy, E_b, of the weakly-bound dimers on the $a > 0$ side of the Feshbach resonance [7–9]. These measurements disagree with our previous measurements based on BEC size. The disagreement in the parameters characterizing the Feshbach parameters is sufficiently large to affect the comparison of the measured Efimov features with universal theory.

In this paper, we report new measurements of E_b, which we fit to obtain $a(B)$. The measurement of E_b has fewer systematic uncertainties than the BEC size measurement, which is affected at large scattering length by beyond mean-field effects and by anharmonic contributions to the trapping potential. The extraction of a from E_b can therefore be more accurate, and unlike the condensate size measurement, E_b is related to a for both thermal gases and condensates. We have measured E_b far enough from the Feshbach resonance that E_b no longer depends quadratically on the detuning of B from resonance, as expected in the universal regime [3, 4]. We show that a commonly adopted correction for non-universal finite range effects, which depends on a single value for the effective range, does not fit the data as well as field-dependent effective range corrections, or a more exact formalism arising from a two-channel model [10]. We use the newly measured and corrected $a(B)$ function to reanalyze our three- and four-body loss data to obtain improved locations of the Efimov

features.

Our experimental methods for producing BEC's and ultracold gases of ^{7}Li have been described in detail previously [6]. Atoms in the $|F = 1, m_F = 1\rangle$ state are confined in an optical trap formed from a single focused laser beam with wavelength of $1.06\,\mu$m. A bias magnetic field, directed along the trap axis, is used to tune a via the Feshbach resonance. For the new data presented here the axial and radial trapping frequencies are $4.7\,$Hz and $255\,$Hz respectively. We adjust the magnetic field to give $a \sim 200\,a_0$, where a_0 is the Bohr radius, and use forced evaporation to produce either ultracold thermal clouds with temperatures of $\sim1.5\,\mu$K, or condensates with condensate fraction that we estimate is greater than 85%. We then adiabatically ramp the field to the desired value and employ *in situ* imaging, either polarization phase-contrast [11] when the density is high, or absorption imaging in less dense clouds.

Atoms are associated into Feshbach molecules by resonantly oscillating the magnetic field at a frequency $h\nu_{\mathrm{mod}} = E_{\mathrm{b}} + E_{\mathrm{kin}}$, where E_{b} is taken to be positive for a bound state, and E_{kin} is the relative kinetic energy of the atom pair [12, 13]. The weakly-bound dimers formed in this way are lost from the trap through collisional relaxation, presumably into deeply-bound vibrational levels [12]. This technique has been used in studies of both homonuclear [12, 14, 15] and heteronuclear [16–18] Feshbach resonances, in addition to the specific hyperfine state of ^{7}Li studied here [7–9].

The oscillating field is produced by a set of auxiliary coils that are coaxial with the bias coils producing the Feshbach field. The amplitude of this field ranges from $0.1\,$G to $0.6\,$G and the duration of modulation ranges from $25\,$ms to $500\,$ms depending on magnetic field. The number of remaining atoms are measured as a function of the frequency of the oscillating field. We find that in the case of a BEC, the loss spectra are fit well by a Lorentzian lineshape. In the case of a thermal gas we fit the loss spectra to a Lorentzian convolved with a thermal Boltzmann distribution [7, 13, 18].

Figure 1 shows characteristic loss spectra at $734.55\,$G (where $a \simeq 1100\,a_0$) for several different temperatures and modulation amplitudes. The Lorentzian component fits to a linewidth of $8\,$kHz, which provides a lower bound on the lifetime of the molecular state of $20\,\mu$s. The temperature extracted from the thermal broadening of the loss feature of the $1.5\,\mu$K data driven with the smallest modulation amplitude of $0.14\,$G agrees within 20% of the measured temperature found by fitting the atomic distribution to a Gaussian. There is no observed thermal broadening of the BEC loss data, as it fits well to a pure Lorentzian. There is no systematic shift in the resonance location with temperature or modulation amplitude, but for large amplitude modulations and sufficiently
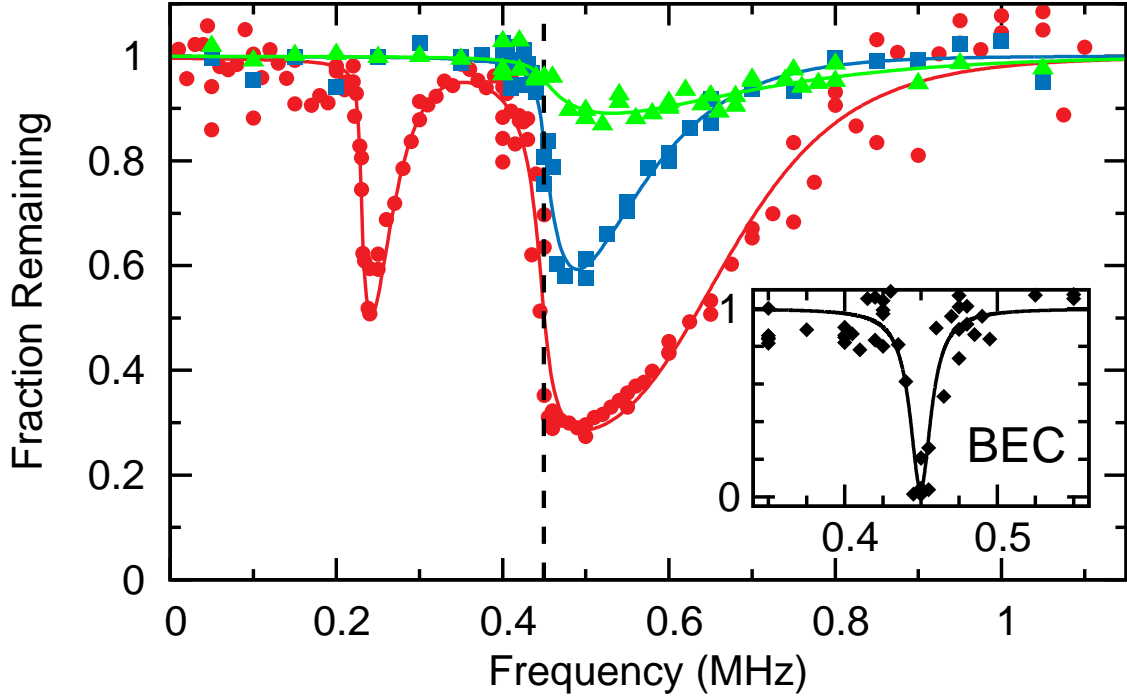
3

FIG. 1. (Color online) Magneto-association induced loss at $B = 734.55$ G, where $a \simeq 1100 \, a_0$. Main plot shows loss spectra for thermal gases with the following modulation amplitudes and temperatures: (▲) 0.57 G and 20 μK, (■) 0.14 G and 1.5 μK, and (●) 0.57 G and 1.5 μK. The solid curves are fits to Lorentzians convolved with thermal Boltzmann distributions. The inset (♦) corresponds to a BEC with a modulation amplitude of 0.14 G. The solid black line is a Lorentzian fit to the condensate resonance and the vertical dashed line in the main figure is the resonance location $E_b/h = 450$ kHz found from this fit.

low temperature we observe a nonlinear resonance at $\frac{1}{2}E_b/h$. No other subharmonics are seen. A similar nonlinear response was reported previously [18].

The results of the measurement of binding energy vs. B are displayed in Fig. 2(a). In the universal regime (see Fig. 2(b)), where a is much larger than any characteristic length scale of the interaction potential, $E_b = \hbar^2/ma^2$, where m is the atomic mass [3, 4]. The solid lines in Fig. 2 show the results of fitting E_b in this universal regime to a, where a is given by the usual Feshbach resonance expression

$$a = a_{bg}\left(1 - \frac{\Delta}{B - B_\infty}\right),\qquad(1)$$

and where a_{bg} is the background scattering length, Δ is the width of the resonance, and B_∞ is the location of the resonance. In the large a universal regime, the first term in Eq. (1) is negligible, and the fit has just two free parameters, B_∞ and the product $a_{bg}\Delta$ (values given in Table I). In this case,

$E_b \propto (B - B_\infty)^2$. In Fig. 2(c) and (d), the same data is recast in terms of $\gamma \equiv (mE_b/\hbar^2)^{1/2}$, where for large a, γ vs. B is a straight line, as is shown in Fig. 2(d). We find no detectable difference in E_b between a BEC or a thermal gas.

Figure 2 suggests that the universal regime extends down to ~725 G, or ~12 G below resonance. Significant discrepancies between the measured E_b and universal theory are observed as the field is decreased further. It is not surprising that the universal regime is only a small fraction of Δ (174 G), since the [7]Li resonance is known to be intermediate between closed-channel and open-channel dominated, as the resonance strength parameter $s_{res} \simeq 0.56$ [19] is neither $\ll 1$ nor $\gg 1$ [4]. For a more precise determination of a it is desirable to extend the analysis into the non-universal regime, where short range attributes of the potential become appreciable. A simple two-channel approach to correct for finite range effects, suggested in Ref. [4] and applied to [7]Li in Refs. [7, 9], is to replace the universal binding energy expression with

$$E_b = \frac{\hbar^2}{m(a - \bar{a} + R^*)^2},\qquad(2)$$

where $\bar{a} = 31\, a_0$ is the mean scattering length [20] (closely related to the van der Waals radius $a_{vdW} = 32.5 a_0$), and $R^* = \bar{a}/s_{res} = 55\, a_0$ is related to the resonance width [21]. The bound state has predominately open channel character only for $a \gg 4R^*$, which is the expected range of validity of Eq. 2 [4]. The best fit to the data using Eqs. 1 and 2 is plotted in Figs. 2.

Although Eq. 2 gives a somewhat better fit to the data than the universal binding energy relation, it clearly fails to represent the entire range of measurements. Higher order corrections to this theory offer little improvement to the overall fit quality [4, 22]. A more complex solution to the two-channel model is given by Eq. 26 in Ref. [10]. This solution is given in terms of R^* and another parameter b, which is related to the van der Waals length and hence, to $\bar{a}$. In order to agree with Eq. 2 in the proper limits, we identify $b = \frac{\sqrt{\pi}}{2}\bar{a}$. Using the previously specified values of R^* and $\bar{a}$, the best fit to the data is shown in Figs. 2. The expected improvement over the simple model (Eq. 2) is borne out, as its range of validity extends to larger detunings from resonance.

The simple two-channel approach represents the effective range of the potential, R_e, with a single value. Since the [7]Li resonance is not open-channel dominated, however, R_e exhibits considerable field-dependence over the width of the resonance. Properly accounting for this field variation should provide a better correction for finite range effects. In order to obtain $R_e(B)$ we numerically solved the full coupled-channels equations using realistic model potentials for both the singlet (closed channel) and triplet (open channel) potentials of the electronic ground state
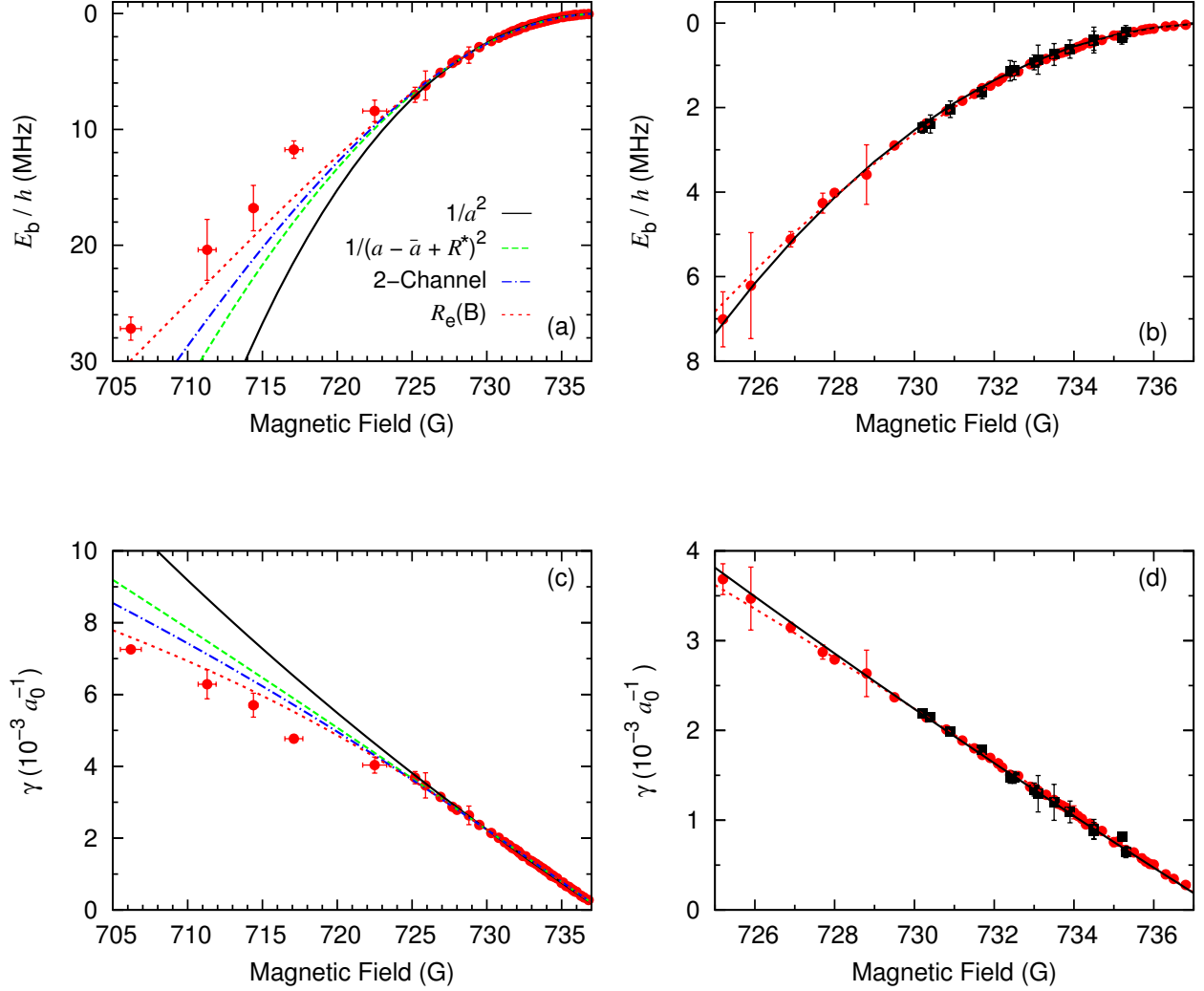
FIG. 2. (Color online) Results of modulation spectroscopy using condensates ($\bullet$) and $1.5\,\mu$K thermal clouds ($\blacksquare$). (a) and (b): E_b vs. B, and (c) and (d): the same data plotted as $\gamma \equiv (mE_b/\hbar^2)^{1/2}$ vs. B. The vertical error bars corresponds to fitting uncertainty, while the horizontal error bars are the shot-to-shot variation of the magnetic field. The solid (black) curves are fits to Eq. (1) using the universal expression $E_b = \hbar^2/ma^2$; the dashed (green) curves are fits using the simple two-channel model, Eq. (2), with the parameters given in the text; the dot-dashed (blue) curves use the solution to the complex two-channel model given in Ref. [10] (Eq. 26), again with parameters as given in the text; and the dotted (red) curves incorporate the field-dependent effective range given in Fig. 3, using Eq. (4). The fits exclude data below 725 G, where $a \simeq 250\,a_0$ is no longer much greater than R^*, and the validity of the non-universal corrections becomes questionable. The resulting Feshbach resonance parameters for the universal model and for the field-dependent effective range are given in Table I. The fitted parameters for the latter are equal to those obtained from the two-channel models, to within experimental uncertainty, for fits constrained to $B \geq 725\,G$.
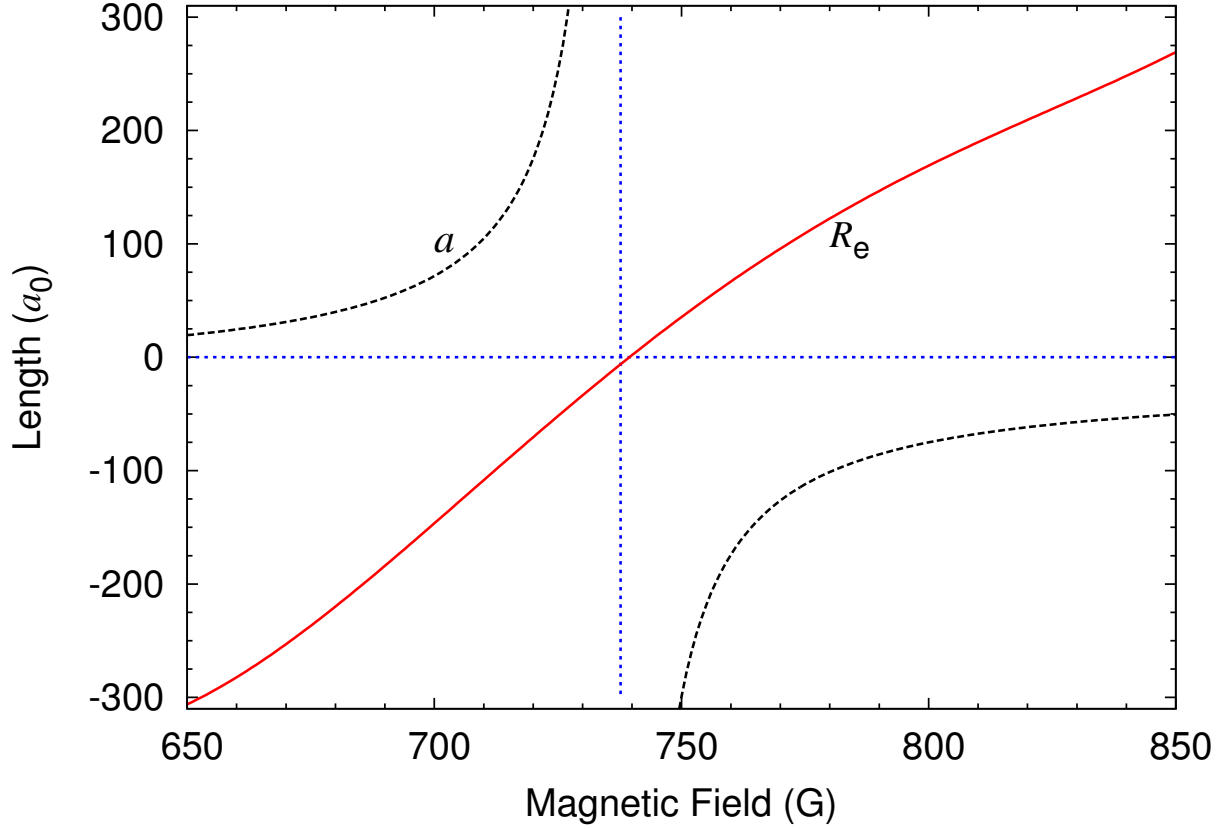
6

FIG. 3. (Color online) Coupled channels calculation of a and R_e for the $F = 1, m_F = 1$ Feshbach resonance in ^{7}Li. The horizontal and vertical dashed (blue) lines indicate $a = 0$ and B_∞, respectively. R_e was fit to a polynomial expansion in the scaled field $b = B - 737.7$ G to obtain $R_e(a_0) = -6.2 + 3.50b - 9.2 \times 10^{-3}b^2 - 6.5 \times 10^{-5}b^3 + 5.7 \times 10^{-7}b^4$.

of Li [23, 24]. These potentials have been refined by adjusting parameters, such as the potential depth and the shape of the inner wall, to give quantitative agreement with experimentally known quantities, which are primarily the locations of Feshbach resonances [6, 8], zero crossings [6], and the binding energies of the least bound triplet molecule [25]. The scattering length and effective range are determined from the energy dependence of the s-wave phase shift δ_0:

$$k \cot \delta_0(k) = -\frac{1}{a} + \frac{1}{2}R_e k^2 + \dots, \tag{3}$$

where $\hbar^2 k^2/m = E_{\text{kin}}$. Figure 3 shows both a and R_e near the Feshbach resonance at 737 G. There is considerable variation in R_e over the width of the resonance, contrary to the assignment $R_e = -2R^*$ [21, 26], or $R_e = 2(\bar{a} - R^*)$ [4]. In comparison, the coupled-channels calculation gives $R_e(B_\infty) \simeq -6\,a_0$. Given this variation, it is not surprising that Eq. 2 does not describe the data well.

The relation between the binding energy of a weakly bound state, or equivalently γ, and a and

Model	B_∞ (G)	Δ (G)	a_{bg} (a_0)	$a_{bg}\,\Delta$ (G a_0)
Universal	737.67(10)	-174	-20.6	3584(60)
Coupled-channels R_e	**737.67(10)**	**-174**	**-19.8**	**3450(60)**

TABLE I. Feshbach resonance parameters obtained by fitting E_b data to Eq. 1 using either the universal model ($\gamma \propto 1/a$) or using Eq. 4 with the coupled-channels calculation of the field-dependent values of R_e. There are large uncertainties in a_{bg} and Δ separately, but their product is well-defined by the data. The choice of Δ was guided by the coupled-channels calculation. The quoted uncertainties reflect shot-to-shot variations in the field and fitting uncertainties. Since the range of validity of the non-universal models is guaranteed only for $R_e \ll a$, data below 725 G is excluded from the fit. In this field range, fits to the two-channel models, the simple one given by Eq. 2 [4], and the more complex solution given by Eq. 26 of Ref. [10], give parameter values that are the same, to within the uncertainties, as the field-dependent R_e model. The parameters from this model, given in bold, are our recommended values.

R_e is given by $\gamma = 1/a + \frac{1}{2}R_e\gamma^2$ [27]. This quadratic equation has one solution with the correct physical behavior for $|R_e/a| \ll 1$ [10, 21, 28]:

$$\gamma = \frac{1}{R_e}\left(1 - \sqrt{1 - \frac{2R_e}{a}}\right). \tag{4}$$

For $|R_e/a| \ll 1$, $\gamma \simeq 1/a\left(1 + \frac{1}{2}R_e/a\right)$. Figures 2(c) and (d) show the results of fitting the measured values of γ to Eqs. (1) and (4). The agreement between theory and experiment is very good over a much larger range of the measurements, and we use this fit to define the Feshbach parameters, which are indicated in bold in Table I. Since $a \gg |a_{bg}|$ for all of the E_b data points, the data is insufficient to separately extract both a_{bg} and Δ. Given the precise knowledge of the location of the field where $a = 0$, $B_0 = 543.6(1)$, found in our previous work [6], a logical choice would be to fix $\Delta = B_0 - B_\infty = -194.1$ G. The coupled-channels calculations, however, offer a useful guide to assigning values to these parameters separately. We find that $\Delta = -174$ G gives a somewhat better fit to the coupled channel results over a larger range in a, so we adopt this value. We stress, however, that the fit to the data strongly constrains the product $a_{bg}\Delta$, but not each parameter separately. A similar procedure was followed in Refs. [7, 8]. Our Feshbach parameters agree with Ref. [9], where they find $B_\infty = 737.8(2)$ G, but slightly disagrees with Ref. [8], which reports $B_\infty = 738.2(4)$ G.

We now turn our attention to the three- and four-body Efimov features previously reported in

Ref. [1]. Figure 4 shows the measured three-body loss rate coefficient L_3 plotted vs. a, where the correspondence between measured values of B is now determined by the new Feshbach parameters given in Table I. While L_3 generally scales as a^4 it is punctuated by several minima and maxima, which are due to Efimov molecular states. The previously reported Efimov maximum a_2^-, corresponding to the second Efimov trimer, is no longer visible because the upward shift in the resonance position by 0.7 G relative to the previous measurement [1] places this feature in the regime where the loss rates are limited by quantum mechanical unitarity [29, 30]. For the same reason, the effect of the second Efimov tetramer associated with the second trimer ($a_{2,2}^T$) is also not visible in measurements of the four-body loss rate coefficient L_4 (not shown). The fitted locations of the remaining features are given in the second column of Table II, where the caption provides a key to the notation. Not all of the features given in Table II are indicated in Figure 4, but expanded views of both L_3 and L_4 are found in Ref. [1].

The origins of three of the features in Table II, indicated by square brackets, are uncertain. The feature a_2^* is nominally located at the atom-dimer resonance where the energy of the second Efimov trimer merges with the atom-dimer continuum. Relatively sharp peaks in $L3$, located near the expected atom-dimer resonance, were previously reported for ^{39}K [38], and ^{7}Li [1, 39]. Since a large dimer fraction is unexpected, a model was developed to explain the presence of enhanced loss even without a large population of dimers [38]. In this model, each dimer produced in a three-body recombination collision shares its binding energy with multiple atoms as it leaves the trap volume due to the enhanced atom-dimer cross section [38]. Recent Monte Carlo calculations, however, conclude that the resulting peak from this avalanche mechanism is too broad and shifted to explain the observations [40]. The remaining two features, $a_{2,1}^*$ and $a_{2,2}^*$, are nominally located at dimer-dimer resonances, where the energy of a tetramer merges with the dimer-dimer threshold [36]. Their assignment also remains tentative, since their observation requires a significant and unsubstantiated dimer population.

The third column in Table II gives the predictions of universal scaling. Pioneering scaling predictions for the three-body [31] and four-body sectors [36, 37], have largely been replaced by the more precise theoretical determinations cited in Table II. Four significant digits are given to reflect the stated precision of the scaling relations. Since the relative positions of all features are expected to be universally connected, the position of only one is needed to completely fix the remaining. We choose the recombination minimum of the second trimer, a_2^+, for this purpose as

9

	Feature	Experiment (a_0)	Universal Scaling in a (a_0)	Universal Scaling in γ (a_0)
$a > 0$	a_1^+	88(4)	61.78*	17.57
	a_2^+	1402(100)	(1402)	(1402)
	$\left[a_2^*\right]$	426(20)	313.5*†‡	293.8
	$\left[a_{2,1}^*\right]$	919(50)	688.5§	680.4
	$\left[a_{2,2}^*\right]$	1902(200)	2127§	2132
$a < 0$	a_1^-	−241(8)	−294.3†	−277.7
	a_2^-	—	−6679†	−6716
	$a_{1,1}^T$	−93(4)	−125.2♯	−75.40
	$a_{1,2}^T$	−235(10)	−268.5♯	−249.6
	$a_{2,1}^T$	−4040(700)	−2841♯	−2857
	$a_{2,2}^T$	—	−6094♯	−6129

References: * [31]; † [32]; ‡ [33]; § [34]; ♯ [35].

TABLE II. Locations of Efimov features, given in units of a_0, of the three- (L_3) and four-body (L_4) loss coefficients. The experimental values of a are extracted from the measured fields using Eq. (1). The horizontal lines indicate features that are too near the resonance to be observed. The estimated uncertainties include fitting uncertainties, as well as the uncertainties in the Feshbach parameters. For $a > 0$, a_i^+ denotes the recombination minimum of the ith Efimov trimer. The origins of three features, labeled as $\left[a_2^*\right]$, $\left[a_{2,1}^*\right]$, and $\left[a_{2,2}^*\right]$, have not been identified, but roughly correspond to expected locations of atom-dimer and dimer-dimer resonances. For $a < 0$, a_i^- denotes the Efimov resonance where the ith trimer merges with the free atom continuum. The remaining features, $a_{i,j}^T$, arise where the jth tetramer associated with the ith trimer merges with the free atom continuum. The final two columns give the predicted locations of the features using universal scaling in a and γ, respectively. The universal scaling relations were obtained from the indicated references. The scaling is anchored by the measured location of a_2^+, which, as an input, is denoted by parentheses. For the last column, the scaling relations are applied to ratios of γ rather than a, and the table entries are the values of a corresponding to these γ.
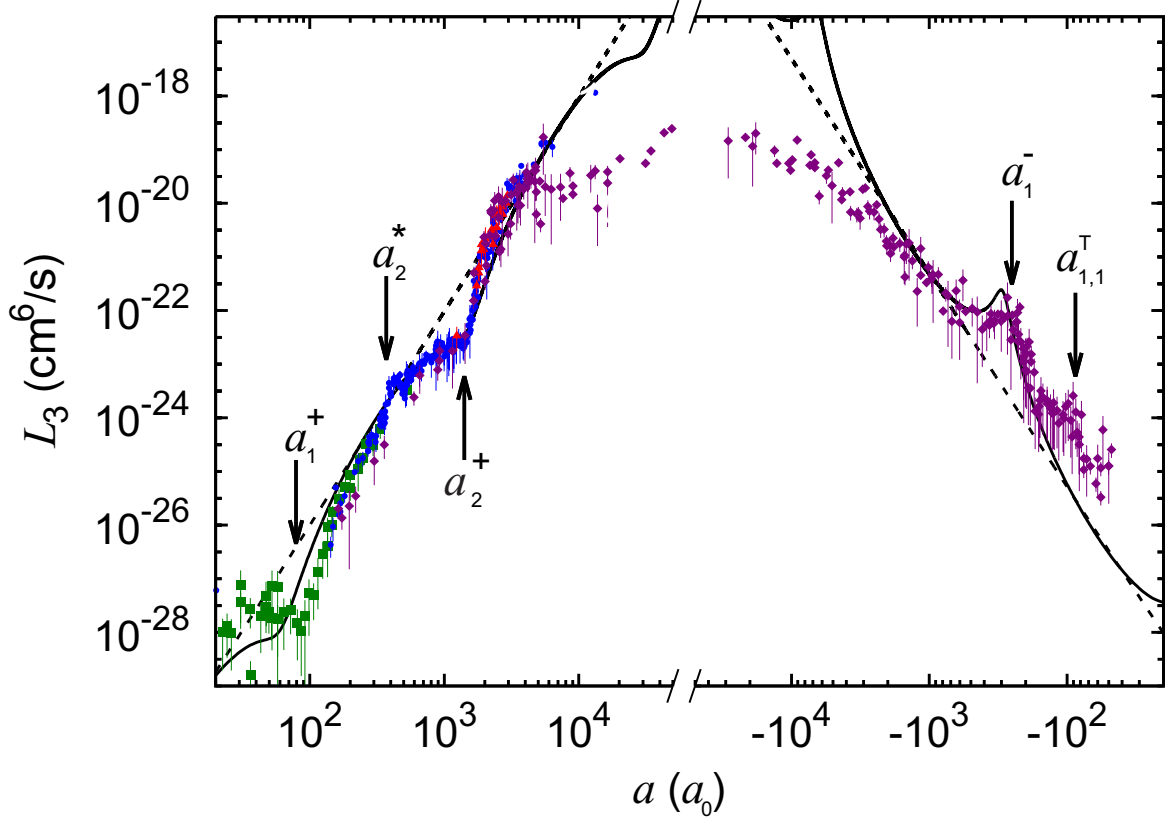
FIG. 4. (Color online) Three-body loss rate coefficient L_3 vs. a. The points are values extracted from the measured trap loss, with the green, blue, red, etc correspond to different trap frequencies, as reported in Ref. [1]. The solid line shows universal scaling in a, where the positions of the features are determined by the single feature a_2^+. The dashed lines show the a^4 scaling in the absence of the Efimov effect. The fitted width parameters are $\eta_+ = 0.038$ and $\eta_- = 0.12$, for the $a > 0$ and $a < 0$ sides of the resonance, respectively.

it is a well-defined feature that occurs at sufficiently large a ($\sim 1400\, a_0$) to be insensitive to short-range effects, while also being small enough in magnitude to not be hypersensitive to B. While the agreement with universal theory of $\sim 30\%$ is good overall, some of the features, in particular a_1^+ and the lowest tetramer $a_{1,1}^T$, occur in the non-universal regime where $|R_e/a|$ is not small. We attempted to correct the universal theory for the effect of finite range using the same strategy applied to the dimer binding energy, that is by applying universal scaling in γ^{-1} (Eq. 4) rather than a. To lowest order, the correction to $1/a$ is $\frac{1}{2}R_e/a^2$. The fourth column in Table II gives these values. We find that such a replacement improves the agreement with experiment for features on the $a < 0$ side of the resonance, but for $a > 0$ the agreement is actually made worse. For the $a > 0$ side of resonance, we note that a correction of opposite sign, corresponding to replacing R_e with $|R_e|$, gives the best

11

agreement. For example, the feature a_1^+ observed at $a = 88\,a_0$ is predicted to be located at $83\,a_0$ under this substitution. The fact that this sign change improves the fit is an empirical observation for which we have no theoretical explanation. We note that an effective field theory for short range interactions has been developed in which corrections to universal scaling of three-body quantities are computed to $O(R_e)$ and that they have been applied to the $F = 1, m_F = 0$ Feshbach resonance in ^{7}Li [41]. It would be interesting to apply the same analysis to the $F = 1, m_F = 1$ resonance to compare with the data presented here.

A measure of universality across the Feshbach resonance may be obtained by evaluating the ratio a_2^+ / a_1^-. Universal scaling in a implies $a_2^+ / a_1^- = -4.76$ [32], whereas experimentally, we find $a_2^+ / a_1^- = -5.82$. We disagree with a previous measurement for the $|F = 1, m_F = 1\rangle$ state in ^{7}Li, which found $a_2^+ / a_1^- = -4.61$ [8, 42]. The discrepancy can be attributed to differences in the measured Feshbach parameters described previously. In addition, the Efimov features observed in Refs. [7, 8] are not as sharp as those reported here, and this may affect the precision for which the location of a feature is extracted. The width is quantified by the fit parameter η, which is related to the lifetime of the Efimov molecule [31]. For Ref. [8], $\eta_+ = 0.17$ and $\eta_- = 0.25$, corresponding to the $a > 0$ and $a < 0$ sides of resonance, respectively, while we find $\eta_+ = 0.038$ and $\eta_- = 0.12$. These large differences, at least in case of η_+, may indicate that η, and hence the dimer lifetime, has an interesting and unexpected temperature dependence, since the $a > 0$ data in Refs. [7, 8] is obtained with a thermal gas, while in our experiment the gas is cooled to nearly a pure Bose condensate.

It was pointed out recently that the location of the first Efimov trimer resonance a_1^-, when scaled by the van der Waals radius a_{vdW}, is remarkably similar for multiple unconnected resonances in the same atom [43], as well as for different atomic species [44]. These observations suggest that there is no need for an additional "three-body parameter" to pin down the absolute positions of the Efimov features, but rather, that this scale is set by short-range two-body physics [44–48]. For the measurements reported here, $-a_1^- / a_{vdW} = 7.42(3)$, which is reasonably close to the range of 8-10 reported in most other cases [43, 44].

The determination of the Feshbach parameters for ^{7}Li in the $|F = 1, m_F = 1\rangle$ state by direct measurement of the dimer binding energy is a significant improvement over our previous measurement using condensate size. Using these more precise parameters we find that the overall agreement between the experimentally determined locations of three- and four-body Efimov features and those obtained from universal scaling is in the range of 20-30%. Since we use the

location of only one feature as input, the agreement strongly supports the contention of universal scaling across the Feshbach resonance. The origin of features nominally located at atom-dimer and dimer-dimer resonances remains an open question. A direct measurement of the equilibrium dimer fraction could help to resolve this issue.

---

[1] S. E. Pollack, D. Dries, and R. G. Hulet, Science **326**, 1683 (2009).

[2] V. Efimov, Phys. Lett. **33B**, 563 (1970).

[3] R. A. Duine and H. T. C. Stoof, Phys. Rep. **396**, 115 (2004).

[4] C. Chin, R. Grimm, P. Julienne, and E. Tiesinga, Rev. Mod. Phys. **82**, 1225 (2010).

[5] T. Kraemer, M. Mark, P. Waldburger, J. G. Danzl, C. Chin, B. Engeser, A. D. Lange, K. Pilch, A. Jaakkola, H.-C. Nägerl, and R. Grimm, Nature **440**, 315 (2006).

[6] S. E. Pollack, D. Dries, M. Junker, Y. P. Chen, T. A. Corcovilos, and R. G. Hulet, Phys. Rev. Lett. **102**, 090402 (2009).

[7] N. Gross, Z. Shotan, S. Kokkelmans, and L. Khaykovich, Phys. Rev. Lett. **105**, 103203 (2010).

[8] N. Gross, Z. Shotan, O. Machtey, S. Kokkelmans, and L. Khaykovich, C. R. Physique **12**, 4 (2011).

[9] N. Navon, S. Piatecki, K. Günter, B. Rem, T. C. Nguyen, F. Chevy, W. Krauth, C. Salomon, Phys. Rev. Lett. **107**, 135301 (2011) (Supplemental Material).

[10] L. Pricoupenko and M. Jona-Lasinio, Phys. Rev. A **84**, 062712 (2011).

[11] C. C. Bradley, C. A. Sackett, and R. G. Hulet, Phys. Rev. Lett. **78**, 985 (1997).

[12] S. T. Thompson, E. Hodby, and C. E. Wieman, Phys. Rev. Lett. **95**, 190404 (2005).

[13] T. M. Hanna, T. Köhler, and K. Burnett, Phys. Rev. A **75**, 013606 (2007).

[14] J. P. Gaebler, J. T. Stewart, J. L. Bohn, and D. S. Jin, Phys. Rev. Lett. **98**, 200403 (2007).

[15] A. D. Lange, K. Pilch, A. Prantner, F. Ferlaino, B. Engeser, H.-C. Nägerl, R. Grimm, and C. Chin, Phys. Rev. A **79**, 013622 (2009).

[16] S. B. Papp and C. E. Wieman, Phys. Rev. Lett. **97**, 180404 (2006).

[17] J. J. Zirbel, K.-K. Ni, S. Ospelkaus, T. L. Nicholson, M. L. Olsen, P. S. Julienne, C. E. Wieman, J. Ye,

and D. S. Jin, Phys. Rev. A **78**, 013416 (2008).

[18] C. Weber, G. Barontini, J. Catani, G. Thalhammer, M. Inguscio, and F. Minardi, Phys. Rev. A **78**, 061601 (2008).

[19] The value of R^* differs from that given in Ref. [4] due the change in Feshbach resonance parameters compared with those given in Ref. [1].

[20] G. F. Gribakin and V. V. Flambaum, Phys. Rev. A **48**, 546 (1993).

[21] D. S. Petrov, C. Salomon, and G. V. Shlyapnikov, Phys. Rev. Lett. **93**, 090404 (2004).

[22] B. Gao, J. Phys. B **37**, 4273 (2004).

[23] E. R .I. Abraham, W. I. McAlexander, J. M. Gerton, R. G. Hulet, R. Côté, and A. Dalgarno, Phys. Rev. A **55**, R3299 (1997).

[24] M. Houbiers, H. T. C. Stoof, W. I. McAlexander, and R. G. Hulet, Phys. Rev. A **57**, R1497 (1998).

[25] E. R. I. Abraham, W. I. McAlexander, C. A. Sackett, and R. G. Hulet, Phys. Rev. Lett. **74**, 1315 (1995).

[26] G. M. Bruun, A. D. Jackson, and E. E. Kolomeitsev, Phys. Rev. A **71**, 052713 (2005).

[27] H. Bethe, Phys. Rev. **76**, 38 (1949).

[28] M. Thøgersen, D. V. Fedorov, and A. S. Jensen, Phys. Rev. A **78**, 020501 (2008).

[29] T. Weber, J. Herbig, M. Mark, H.-C. Nägerl, R. Grimm, Phys. Rev. Lett. **91**, 123201 (2003).

[30] J. P. D'Incao, H. Suno, and B. D. Esry, Phys. Rev. Lett. **93**, 123201 (2004).

[31] E. Braaten and H.-W. Hammer, Phys. Rep. **428**, 259 (2006).

[32] K. Helfrich, H.-W. Hammer, and D. S. Petrov, Phys. Rev. A **81**, 042715 (2010).

[33] A. O. Gogolin, C. Mora, and R. Egger, Phys. Rev. Lett. **100**, 140404 (2008).

[34] A. Deltuva, Phys. Rev. A **84**, 022703 (2011).

[35] A. Deltuva, Phys. Rev. A **85**, 012708 (2012).

[36] J. P. D'Incao, J. von Stecher, and C. H. Greene, Phys. Rev. Lett. **103**, 033004 (2009).

[37] J. von Stecher, J. P. D'Incao, and C. H. Greene, Nature Phys. **5**, 417 (2009).

[38] M. Zaccanti, B. Deissler, C. D'Errico, M. Fattori, M. Jona-Lasinio, S. Müller, G. Roati, M. Inguscio, and G. Modugno, Nat. Phys. **5**, 586 (2009).

[39] O. Machtey, D. A. Kessler, and L. Khaykovich, Phys. Rev. Lett. **108**, 210406 (2012).

[40] C. Langmack, D. Hudson Smith, and E. Braaten, arXiv:1205.2683 (2012); *Ibid*. arXiv:1209.4912 (2012).

[41] C. Ji, D. R. Phillips, and L. Platter, Europhys. Lett. **92**,13003 (2010); *Ibid*. Ann. Physics **327**, 1803 (2012).

[42] The notation, a_+ and a_-, in Refs. [7, 8] differs from ours: $a_2^+ = 4.764\,a_+$ and $a_1^- = a_-$. Furthermore, the universal ratio given as $a_+/a_- = 0.96$ in those references should be updated to 1.0, according to Ref. [32].

[43] M. Berninger, A. Zenesini, B. Huang, W. Harm, H.-C. Nägerl, F. Ferlaino, R. Grimm, P. S. Julienne, and J. M. Hutson, Phys. Rev. Lett. **107**, 120401 (2011).

[44] C. Chin, arXiv:1111.1484 (2011).

[45] J. Wang, J. P. D'Incao, B. D. Esry, and C. H. Greene, Phys. Rev. Lett. **108**, 263001 (2012).

[46] R. Schmidt, S. P. Rath, and W. Zwerger, Eur. Phys. J. B **85**, 386 (2012).

[47] P. K. Sørensen, D. V. Fedorov, A. S. Jensen, and N. T. Zinner, Phys. Rev. A **86**, 052516 (2012).

[48] P. Naidon, S. Endo, and M. Ueda, arXiv:1208.3912 (2012).